Energy and angle resolved SIMS studies of CO on Ni(001)

R. A. Gibbs,[a] S. P. Holland,[b] K. E. Foley, B. J. Garrison,[c] and N. Winograd

Department of Chemistry, The Pennsylvania State University, University Park, Pennsylvania 16802
(Received 27 May 1981; accepted 8 September 1981)

Energy and angle resolved secondary ion mass spectra (SIMS) for CO chemisorbed on Ni(001) have been examined in detail. This system has been chosen as a model since it provides intense secondary ion yields and since the original surface geometry of the adsorbed CO is known by other techniques. Theoretical curves for the ejected atomic and molecular species have been generated using a classical dynamics procedure for computing the momentum dissipation of the 1000 eV incident Ar^+ ion. We found that for Ni^+ ion ejection the results agreed well with calculated spectra of the neutral particles where the CO is placed in a linear bonded site, if the neutral atom trajectories were modified by inclusion of an image force. The agreement was excellent for polar angle, azimuthal angle, and secondary particle kinetic energy distributions. Similar agreement was found for Ni_2^+ and $NiCO^+$ species although the statistical reliability of the calculated curves was not as high as for the Ni^+ species. The results provide convincing evidence that the classical dynamics model can provide a semiquantitative insight into the SIMS process. In addition, the presence of a relatively strong image force indicates that the ion must be formed very close to the surface. Finally, since agreement between theory and experiment was found over a wide range of conditions, the results suggest that the ionization probability of the ejecting particle is isotropic and only weakly dependent on particle velocity. These criteria impose a number of constraints on possible theories of ionization mechanisms.

I. INTRODUCTION

Recently there has been considerable interest in utilizing kilovolt ion beams to characterize the chemistry of simple gas molecules bonded to well-defined metal surfaces.[1-6] This characterization is possible since various types of atomic and molecular ions are observed to eject from an ion bombarded solid, and it is believed that the nature of these species reflects in a systematic way the original surface environment. The physical basis of the process is that momentum exchange between the primary ion and the atoms in the lattice initiates a tremendous amount of atomic motion. Some of the moving atoms obtain a sufficient component of momentum oriented into the vacuum that they are able to overcome the surface binding forces and eject from the solid. A fraction of these particles are ionized as they leave the surface and can, therefore, be detected directly with a mass spectrometer (i.e., as in secondary ion mass spectrometry of SIMS). A number of important aspects have been gleaned from existing experimental studies. For CO adsorbed on Ni, for example, the presence of ejected $NiCO^+$ with only minor NiC^+ and NiO^+ ions is indicative of molecular, rather than dissociative adsorption.[1-4] Other workers also have proposed that the ejected Ni_2CO^+ ion is indicative of a bridge bonded CO structure while the $NiCO^+$ species originates from a linear bonded species,[3] although this interpretation has been questioned.[2,4]

The high sensitivity of SIMS to the top layer of a solid and the large amount of data present in the spectra make SIMS a potentially powerful tool for surface studies. The lack of a cohesive theory to quantitatively describe the secondary ion emission process, however, has been a major factor in slowing attempts to effectively utilize the spectral information. It appears there are two major stumbling blocks which need to be removed before such a theory can be developed. First, the nuclear motion of the lattice atoms induced by the primary ion must be determined as momentum is dissipated by the sample. Second, the mechanism and probability of the ionization of the ejecting particles must be somehow incorporated into the dynamics process.

It now appears feasible to solve the first part of the problem using a classical dynamics procedure that has been under development for several years.[7-13] With this model, the ejection of neutral atoms (sputtering) has been successfully predicted and compared with experimental results for a number of situations. These include relative yields as a function of single crystal face,[7] secondary particle kinetic energy,[13] adsorbate exposure,[9] and azimuthal ejection angle.[10] The formation of clusters is also an integral part of the model.[12] Of particular interest here is the proposal that the ejection direction of either the monomers or clusters reflects the original bonding geometry of the surface species.[10,14] The problem of ionization is more complex although a new microscopic quantum mechanical scheme which incorporates the electronic structure of the substrate is currently under development.[15] The approach is readily cast into the framework of the classical dynamics model. At this point, however, sufficiently well-defined experimental measurements are not available to directly compare to theoretical yields.

In this work we report the results of a detailed study of the angle, energy, and mass dependence of secondary ion emission for a Ni(001)c(2×2)–CO surface. The objective of this study is to provide sufficiently well-resolved data such that direct comparisons between the calculated neutral atom trajectories and the measured ion trajectories can be made. To carry out this goal, we have constructed a SIMS spectrometer that incorporates an electrostatic sector and quadrupole mass filter for energy and mass analysis. In addition, this

[a] Present address: Westhollow Research Center, Shell Development Company, Houston, TX 77001.
[b] Present address: IBM, General Technology Division, Essex Junction, Vermont 05452.
[c] Alfred P. Sloan Research Fellow.

 0021-9606/82/010684-12$02.10

detector can be rotated under ultrahigh vacuum conditions, allowing variations of the polar collection angle of secondary ions. The crystal can also be rotated for measurement of ion intensities as a function of azimuthal angle. As a model we have chosen the Ni(001)c(2 ×2)–CO system since it provides very intense secondary ion signals and its bonding geometry and electronic structure have been examined by a wide range of methods including a detailed LEED analysis. Further, the classical dynamics procedure for calculating trajectories on this system have been recently developed.[18]

We find that for Ni^+ ion ejection the results agree well with calculated spectra for the neutral particles for CO placed in a linear bonded site, if the neutral atom trajectories are modified by inclusion of an image force. The agreement is excellent for polar angle, azimuthal angle, and secondary particle kinetic energy distributions. The global correlation between experiment and theory suggests that a straightforward relationship exists between neutral and ion trajectories. Another consequence is that the ionization probability is at most only weakly dependent on particle velocity and ejection direction. These aspects of the surface ionization process place severe constraints on any proposed theoretical models. Further, the results are reasonably sensitive to the bonding geometry chosen for the chemisorbed CO. For example, calculations using a twofold bridge bonding site yield poor agreement with the measured azimuthal plots. Other experiments with Ni_2^+ and $NiCO^+$ species show only qualitative agreement with theory, probably due to the limited statistical reliability of the calculated cluster yields. In general, we feel the results provide a good basis to describe the particle ejection process for metals reacted with simple molecules. The sensitivity of the results to bonding geometry indicates that this approach may become a valuable surface structural probe.

II. EXPERIMENTAL ASPECTS

The angle resolved SIMS measurements are performed using a specially designed UHV chamber such that the quadrupole mass filter (Riber AQX156) can be rotated with respect to the primary ion beam. This feature is achieved using a set of three 56 cm differentially pumped Teflon seals.[17] A manipulator for the crystal then provides azimuthal rotation, heating to 1300 K, cooling to 175 K, and vertical translation to a LEED apparatus located on a different level in the chamber. The secondary ions are then angle and energy selected using a 90° spherical electric sector in front of the mass analyzer. The calculated polar angle resolution, based on the size of the apertures and the field-free distance from the sample to the lens, is estimated to be ± 7°. The azimuthal angle resolution $\Delta\phi$ can be approximated from the polar angle θ, since $\Delta\phi \simeq \Delta\theta/\sin\theta$. Using a zoom lens arrangement, the bandpass of the analyzer can be varied from approximately 2 eV for recording energy spectra to nearly 15 eV for obtaining maximum sensitivity. Details of the apparatus are available elsewhere.[18]

The Ni(001) crystal was cleaned and annealed in accord with a standard surface preparation procedure.[1] The SIMS analysis taken at a beam current of 1×10^{-9} amps/cm^2 showed no O^+, O_2^+, C^+, or C^-, and only small amounts of O^- and $NiOH^+$ as expected from earlier studies.[1] The annealed crystal exhibited sharp LEED spots indicative of the ordered (001) orientation. Upon exposure of the crystal to 2L CO, the Ni^+ peak reached a reproducible plateau, corresponding to the c(2×2) coverage.[1,19,20] Base pressure in the experimental chamber was 1×10^{-10} Torr, but due to leaking of Ar from the ion gun, the chamber pressure rose to ~1×10^{-9} Torr during SIMS experiments. The total primary ion dose during the experiments was kept below 10^{13} ions/cm^2 to minimize surface damage, consistent with a $NiCO^+$ peak intensity decrease of less than 10%. The primary ion beam was fixed at normal incidence relative to the sample. All experiments were performed at a sample temperature of 295 ± 2 K.

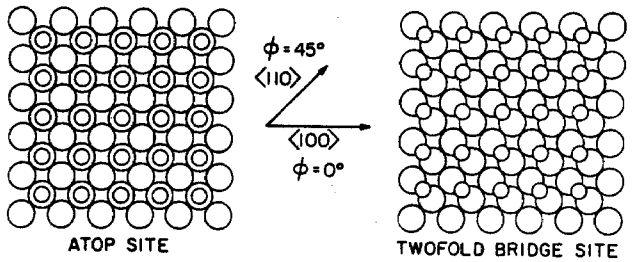

FIG. 1. Model surface structures used in the classical dynamics computations. The left side of the figure depicts the Ni(001) surface with Ni atoms represented by the large circles and the CO molecules adsorbed in atop sites represented by the smaller circles. The right side of the figure depicts the Ni(001) surface with CO adsorbed in twofold bridge sites. The azimuthal directions used in this paper are defined in the inset.

In all of these experiments, the angle θ is measured with respect to the surface normal, with the angle $\phi = 0°$ defined along the ⟨100⟩ directions as shown in Fig. 1. Azimuthal spectra are obtained by rotating the single crystal over 200° about the primary beam axis, and the data are normalized to the maximum peak intensity and properly symmetrized. No other smoothing or background subtraction techniques are employed. Energy spectra are not corrected for contact potential differences between the sample and the analyzer. For the comparisons with theory, the calculated and experimental peak maxima are matched, which amounts to shifting the experimental spectra by ~3 eV to lower kinetic energy.

III. THE CALCULATION

The angular distributions of particles that eject due to the ion bombardment process are predicted by a classical dynamics model. First, a microcrystallite is constructed with the metal and adsorbate atoms in their initial geometries. The motion of all these particles plus the bombarding ion is developed in time by integrating Hamilton's equations of motion. From the final momenta of the ejected particles, the energy and angles of ejection can be determined.

The systems of interest in this study are Ni(001) and

Ni(001) with a c(2×2) overlayer of CO. From LEED studies[21,22] the CO is thought to bond in atop or linearly bonded sites with the carbon atom 1.76 Å above the nickel atom as shown in Fig. 1. We have chosen to model both this configuration and one where the CO molecule is situated in a twofold bridge site. We have limited these studies to the case were the Ar^+ ion bombard the crystal at normal incidence with 1000 eV of energy. A complete description of the dynamics procedure has been published elsewhere[7–12,16,23] with the details relevant to the CO–Ni system given in Ref. 16.

The calculated ejection energies and angles of the atoms will be compared to the experimental data. Instead of plotting histograms we have chosen to approximately convolute the experimental resolution into the calculated results. For example, for azimuthal data the points are spaced quite closely in ϕ with the intensity at each point representing the number of particles with an azimuthal angle in the range $\phi \pm \Delta\phi/2$. In many of our previous theoretical studies, the calculation of 50–200 Ar^+ ion impacts at various points on the surface was sufficient to predict statistically reliable observables. For the comparisions to the angular distributions presented in this study, many more ion impacts are needed. Given in Table I is a summary of the results of the calculations. Even though 1255 Ar^+ ion impacts result in almost 6000 atoms that eject from the clean nickel surface, in some cases the number of atoms that are traveling in a specific direction within a given energy range may be too small to make statistically meaningful comparisons to experiment.

IV. RESULTS AND DISCUSSION

Static SIMS spectra resulting from 1000 eV Ar^+ ion bombardment of the Ni(001)c(2×2)–CO surface are shown in Fig. 2. The spectrum obtained from secondary ions of 3±2 eV exhibits small impurity peaks at m/e 39 (K^+) and 75–77 ($NiOH^+$) in addition to the expected Ni^+, $NiCO^+$, Ni_2^+, and Ni_2CO^+ peaks. Notice, however, that the $NiCO^+/Ni^+$ ratio is ~1.4, in contrast to previously reported values of 0.22[1] and 0.6.[2,4] We ascribe these apparent discrepancies to differences in the secondary ion energy acceptance range, resulting in differing collected percentages of the integrated secondary ion energy distribution.[2] The data shown in Fig. 2(b), taken with a secondary ion kinetic energy of 13±2 eV, demonstrate this point. The K^+, $NiCO^+$, and Ni_2CO^+ species, which have a very narrow energy distribution that peaks at low kinetic energies, are completely absent, and the $NiOH^+$ and Ni_2^+ peaks have been substantially attenuated. The Ni^+ ion, on the other hand, actually shows increased intensity in the higher secondary ion kinetic energy range spectrum. As will be discussed later, this result is a manifestation of the higher peak energy and breadth of the Ni^+ secondary ion energy distribution at this polar angle.

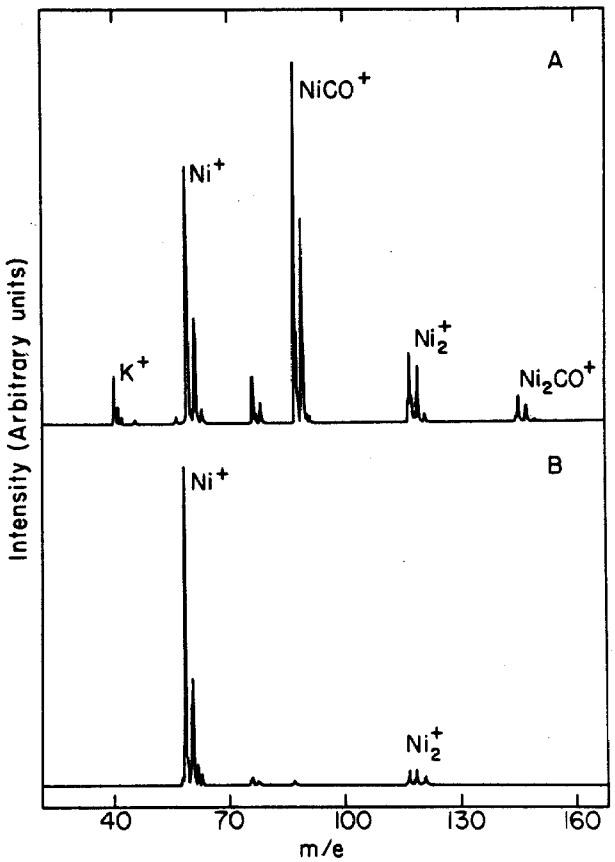

FIG. 2. Secondary ion mass spectra of Ni(001)c(2×2)–CO. Spectrum (a) was recorded at $\theta = 60°$, $\phi = 0°$ with a secondary ion kinetic energy of 3±2 eV. Spectrum (b) was recorded under the same conditions except that only ions of 13±2 eV kinetic energy were detected. The Ar^+ ion was directed to the sample at normal incidence with 1000 eV kinetic energy.

TABLE I. Number of particles ejected due to 1000 eV Ar^+ ion bombardment of Ni(001) and Ni(001)c(2×2)–CO at normal incidence.

		Ni(001)c(2×2)–CO	
	Ni (001)	Atop site	Twofold bridge site
Ar^+ ion impacts	1255	1450	841
Ni ejected	5842 (4.65)[a]	3803 (2.62)	2922 (3.47)
CO ejected	•••	4314 (2.98)	3504 (4.17)
Ni_2 ejected	216 (0.17)	60 (0.041)	67 (0.080)
NiCO ejected	•••	353 (0.24)	273 (0.32)

[a]The number in parentheses is the average yield per incident ion.

In the remainder of this section, we will present detailed measurements of the secondary ion intensity vs primary (Subsec. A) and secondary ion energy (Subsec. B), polar angle θ and azimuthal angle ϕ (Subsec. E). In addition, we will comment on the relationship between neutral and ion trajectories (Subsecs. C and D) and will present preliminary results for the clean Ni(001) surface (Subsec. E) and for the ejected clusters from Ni(001)c(2×2)–CO (Subsec. F). Finally, we will indicate the sensitivity of the results to the assumed bonding geometry of the adsorbed CO. The focus of the analysis of these results will be on the comparison between observed energy and angular distributions and the pre-

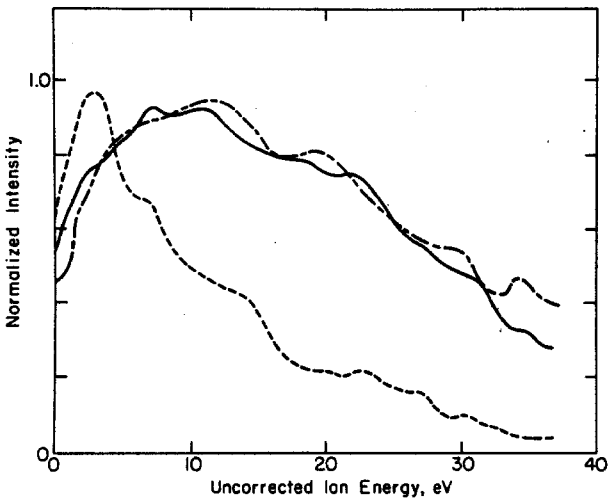

FIG. 3. Uncorrected secondary ion kinetic energy distributions for Ni^+ ion ejected from Ni(001)c(2×2)–CO. The distributions were recorded at $\theta = 45°$ and $\phi = 0°$ using an energy bandwidth of ~4 eV FWHM. The curves were produced by bombarding the solid with Ar^+ ions at normal incidence with kinetic energies of 1500 eV (——), 1000 eV (— - — -), and 300 eV (- - - - -).

dictions of the molecular dynamics calculation, with the hope of gaining information about both the structural sensitivity of the technique and the fundamental ionization processes operative in secondary ion emission.

A. Effect of primary ion energy

Although it has long been appreciated that secondary ion yields are a function of primary ion energy, there have been few experiments specifically designed to achieve a fundamental understanding of the observed effects, particularly in the low energy (<2000 eV) regime. Wittmaack[24] noted a strong energy dependence of secondary ion yields for primary ions in the 2–15 keV range which could not be completely ascribed to either variation in the calculated sputtering yield or differences in secondary ion energy distributions. Other workers have noted variation in secondary ion yield ratios[2,25] and in secondary ion energy distributions[25–28] as a function of primary ion energy within the low energy range.

In the context of the present experiment, the effect of primary ion energy is noted primarily in the energy spectra of secondary ions and to a lesser extent in the azimuthal spectra. In Fig. 3, we show Ni^+ secondary ion energy spectra obtained from Ar^+ bombardment of Ni(001)c(2×2)–CO at 300, 1000, and 1500 eV for $\theta = 45°$ and $\phi = 0°$. The 1000 and 1500 eV curves are essentially identical and are in qualitative agreement with the energy distribution observed by Sroubek for Ni^+ ions ejected from clean polycrystalline nickel bombarded by 2.5 keV Ar^+ ions.[25] However, decrease of the primary ion energy to 300 eV shifts the maximum from ~15 to 6 eV with concurrent peak narrowing, again in accord with previous results.[25] Secondary ion energy spectra obtained at ejection angles of $\theta = 30°$, 60°, and 75° (all at $\phi = 0°$) show similar trends as the primary ion energy is reduced, although the observed change at $\theta = 75°$ is not as dramatic since the energy distributions are initially much narrower than the $\theta = 45°$ curve. The interpretation of these results is that lower kinetic energy primary ions do not have sufficient momentum to completely initiate the collision cascade of atoms within the solid. The secondary ion kinetic energy distribution is therefore strongly peaked at low energies and does not possess a high energy tail. Once the cascade is fully developed, however, the process becomes nearly independent of the source of the energy deposition[28] and the intensity dies off rather slowly at high kinetic energies. As we shall see in subsequent sections, this trend is nicely predicted by the classical dynamics calculations.

Interpretation of the results for the azimuthal spectra is not so straightforward. The anisotropy observed in Ni^+ azimuthal spectra from Ni(001)c(2×2)–CO is slightly greater for 300 eV Ar^+ bombardment than for 1500 eV bombardment at all polar angles studied. Apparently, at lower primary ion energies, there are fewer ejection mechanisms that contribute to the total yield and the results are therefore more sensitive to the arrangement of surface atoms. It should be noted that for azimuthal spectra obtained at primary ion energies between 1 and 5 keV that the anisotropies in the azimuthal plots are virtually identical. Although a more thorough study is needed to substantiate this conclusion, it is in accord with previous experiments[2,5] and preliminary results of a detailed molecular dynamics calculation of primary ion energy effects on the Ni–CO system.[29]

B. Effect of secondary ion energy

The magnitude of the secondary ion kinetic energy is a critical parameter which strongly influences the angular spectra of secondary ions. In Fig. 4 we show the

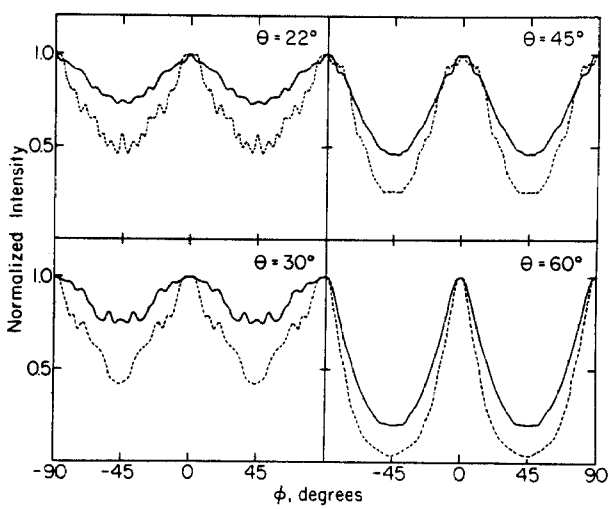

FIG. 4. Dependence of Ni^+ ion yield on azimuthal angle at various polar angles. The curves were obtained by bombarding with 1000 eV Ar^+ ions at normal incidence. The solid lines (——) represent data recorded by selecting secondary ions with 3±3 eV kinetic energy while the dashed lines (- - - - -) represent data recorded at 16±4 eV kinetic energy.

azimuthal angular dependence of Ni^+ ion intensity for secondary ions ejected from Ni(001)c(2×2)–CO at $\theta = 22°$, 30°, 45°, and 60° by 300 eV Ar^+ ions. The upper (solid) curve in each panel corresponds to secondary ions of 3 ± 3 eV, the lower (dashed) curve to secondary ions of 16 ± 4 eV. In each case the minimum intensity ($\phi = \pm 45°$) is considerably less on the normalized scale for the high kinetic energy secondary ions, a trend that is found to be true regardless of primary ion energy, secondary ion species, or polar angle. This result is in qualitative agreement with the results of the molecular dynamics calculations,[10] which indicate that low energy particles tend to eject after much of the momentum of the primary ion has dissipated within the crystal and destroyed much of the initial surface order. High kinetic energy particles, on the other hand, leave the crystal after only a few collisions have occurred, and thus more accurately reflect the symmetry of the surface. The maximum intensity at $\phi = 0°$ is due to the relative lack of obstruction encountered by a particle ejecting in the ⟨100⟩ directions, corresponding to the fourfold "holes" between nearest-neighbor nickel atoms on the (001) face. Particles initially directed along the ⟨110⟩ directions ($\phi = 45°$), however, tend to be scattered by these nearest-neighbor atoms. The effect becomes more pronounced at high polar angles, leading to the increased anisotropy as the polar angle is increased from 22° to 60°. Since the trend is a manifestation of the underlying surface structure, it is predicted to be general for all (001) face centered cubic metals. The effect has been previously observed to be true for metal ions ejected at $\theta = 45°$ from clean Ni(001)[30] and Cu(001)c(2×2)–O.[14] Similar influences of surface structure have been noted in polar spectra, to be discussed in the following sections.

C. Effect of ionization on secondary particle trajectories

One of the main goals of the energy and angle resolved SIMS experiments is to gain a fundamental understanding of the physical processes which ultimately lead to the detection of a secondary ion. We begin with the assumption that the energy and angular distributions of neutral particles ejected from the sample are accurately described by the dynamics procedure within the limits imposed by imperfect knowledge of the relevant interaction potentials. Any differences between the observed secondary ion and predicted neutral particle behavior must therefore be either a manifestation of the ionization process itself or indicative of secondary ion trajectory modification due to ion-surface interactions.

We have investigated two explicit functional forms of the energy and angular dependence of the ionization probability R^+ by comparing our measured results for ions to the calculated neutral atom yields. Here, R^+ is defined as the ratio of the number of ejected ions to the number of ejected neutral atoms. The first form is a result of early theoretical studies of secondary ionization which assumes that particles leave the surface in the form of ions.[31,32] Some of these ions are subsequently neutralized by either Auger processes or resonant tunneling.[33] The ionization probability R^+ is a function of ion velocity as[34]

$$R^+ \alpha \exp(-A/av_\perp) , \tag{1}$$

where A is the Auger transition rate at the surface, a is a critical distance, and $v_\perp$ is the perpendicular velocity component of the ejecting ion. Values of A/a from 2.5×10^5 to 2×10^6 cm/s have been reported.[35] The unrealistically high velocity dependence of R^+ predicted by this model[36] as well as the physically unsatisfactory application of bulk band structure approximations at the ejection site[37] have been pointed out by other workers. In addition, we find that energy and polar angle spectra observed in this study cannot be reconciled with the predicted neutral particle distributions using the correction from Eq. 1 alone, regardless of the assumed value of A/a.

In the second case, we assume that R^+ is independent of both secondary particle energy and ejection angle. This assumption is consistent with a recent theoretical study[15] which is in general agreement with the observed energy and ionization potential dependence of R^+, and which predicts only slight changes in R^+ over the secondary ion energy range studied in this work. However, if R^+ is energy and angle independent, then neutral and ionized particles should exhibit identical energy and angular distributions, which we find not to be the case.

Since the predicted neutral distributions cannot be made to fit the ion distributions with either of the assumed functional forms of R^+ alone, we next consider the effect on the secondary ion trajectories due to interaction between the leaving ion and the crystal surface. It has been suggested that the interaction between a metallic surface and a relatively slowly moving ion can be approximated using the classical method of images.[38] To our knowledge, however, the image force correction has never been explicitly included in comparison of neutral and ionic particle trajectories and has only occasionally been discussed in relation to ionization theories.[39] We find that modification of the neutral particle trajectories due to the image force experienced by the leaving ion results in excellent agreement with the energy and angle resolved SIMS experiments if R^+ is assumed to be isotropic and energy independent. The image force is a consequence of the attraction between the leaving ion and an equal charge of opposite sign created in the polarizable electron distribution of the metal which acts to reduce the perpendicular velocity component of the leaving ion. The magnitude of the image force is related to the distance of the leaving particle from the image plane as it acquires net charge in the ionization process. Since neither the timescale of ionization relative to the motion of the secondary particle nor the exact nature of the image plane during the ejection process is known, the image force is treated as an adjustable parameter for a given substrate-ejected particle combination. If θ_n is the polar angle of the atom's velocity vector at the instant of ionization, the ion emerges with a final direction given by

$$\theta_i = \tan^{-1}\left[\frac{E_0 \sin^2\theta_n}{E_0 \cos^2\theta_n - E_{\text{image}}}\right]^{1/2} , \tag{2}$$

where θ_i is the corrected polar ejection angle of the leaving ion, E_0 is the kinetic energy of the neutral par-

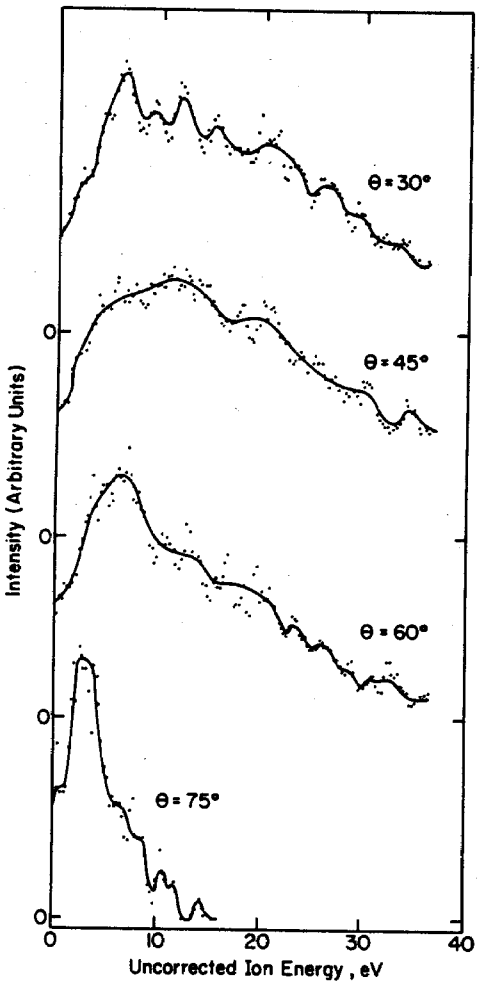

FIG. 5. Uncorrected secondary ion kinetic energy distributions of Ni^+ ions ejected at various polar angles from Ni(001)c(2×2)–CO by 1000 eV Ar^+ ions.

ticle ejected at polar angle θ_n, and E_{image} is the perpendicular energy correction resulting from the work needed to overcome the image force. For simplicity, if we assume that the leaving particle instantaneously acquires a unit charge in the process of ionization, then E_{image} may be expressed as

$$E_{image} = e^2/4z = 3.6\,\text{eV}/a_0\ , \tag{3}$$

where a_0 is the height in angstroms of the particle above the image plane at the instant of ionization and is a convenient measure of the magnitude of the image force. We find that values of 1.0 Å (E_{image} = 3.6 eV) for Ni^+ ejected from Ni(001)c(2×2)–CO and 1.5 Å (E_{image} = 2.4 eV) for Ni^+ ejected from clean Ni(001) yield the best agreement between experiment and theory.

The expression given in Eq. (2) is only valid when the denominator of the argument is positive. If E_{image} is greater than the perpendicular component of the particle energy, the leaving ion will not escape the image potential field. Thus, the effect of the image force is to create an energy and angle dependent potential barrier which must be surmounted as the ion leaves the surface. It is implicitly assumed in Eq. (2) that E_{image} is constant with respect to E_0 and θ_n. We also note that for the relatively high values of E_{image} found in this investigation, the van der Waals interaction between the leaving neutral molecule and the surface before ionization may be justifiably neglected. Although the interaction energy of the ion and image charge reaches some saturation value at low a_0 values,[40] we have neglected explicit treatment of this problem since the electron density distribution at the ejection site is unknown.

D. Comparison of calculated and observed energy distributions

The energy distributions of secondary ions are strongly perturbed by the image force since it affects slow moving particles much more strongly than fast moving particles. In Fig. 5 we show the observed energy distributions of Ni(001)c(2×2)–CO bombarded by 1000 eV Ar^+ ions measured at $\theta = 30°$, 45°, 60°, and 75° at $\phi = 0°$. The polar angular resolution is estimated to be ~14° FWHM with the azimuthal angular resolution given by

$$\Delta\phi = \Delta\theta/\sin\theta\ . \tag{4}$$

Each spectrum was obtained with a primary ion dose of 10^{12} ions/cm^2, resulting in an acceptable signal-to-noise ratio at the ~4 eV FWHM energy bandwidth setting.

In Fig. 6 we compare each of the Ni^+ ion energy distributions obtained at various polar angles to the calculated spectra and to the calculated spectra corrected for the presence of the image force. It is initially apparent that the calculated energy spectra for the neutral particles are more concentrated at lower kinetic energies than are the measured Ni^+ ion distributions. This difference has been noted previously in many studies. For example, for 1 keV Ar^+ on Cu, the ion energy distribution peaks at 4 eV and tails off as $E^{-0.5}$, while the neutral distribution peaks at 3 eV and tails off as roughly E^{-2}.[28] When the Ni atom distributions are corrected by

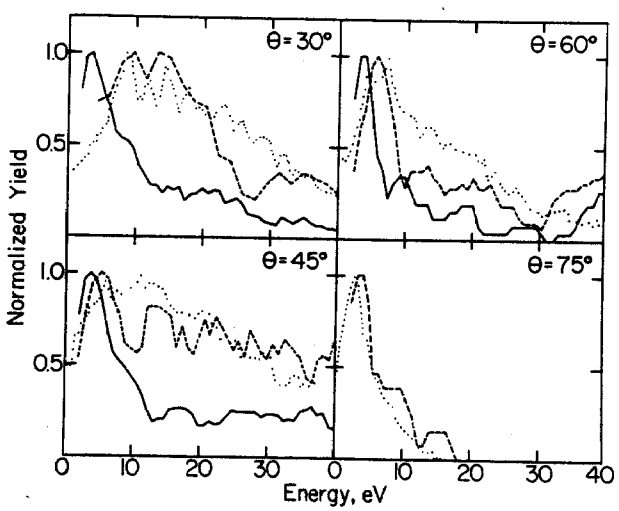

FIG. 6. Energy distributions for Ni ejected from Ni(001)c(2×2)–CO due to bombardment by 1000 eV Ar^+ ions at normal incidence. The three curves in each panel are identified as follows: (——) calculated Ni distribution, (- - - - -) calculated Ni distribution with inclusion of the image correction and (· · · · ·) experimental points for Ni^+. In each case, $\phi = 0°$.

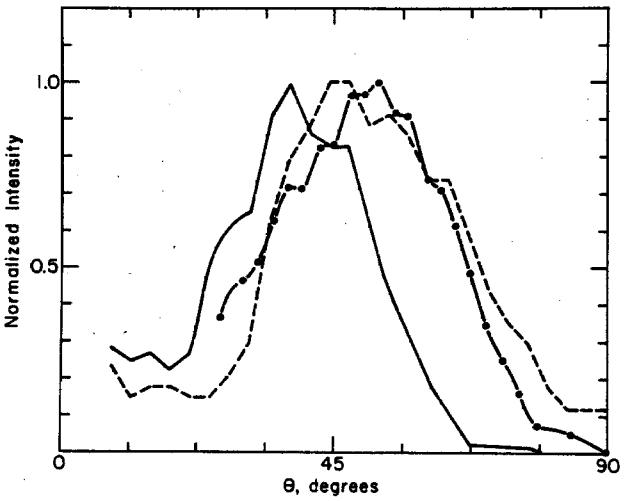

FIG. 7. Polar angle distributions for Ni ejected from Ni(001)c(2×2)–CO. Experimental conditions and codings are the same as for Fig. 6. The curves are recorded by selecting only those particles with 7±2 eV kinetic energy.

an $E_{image}=3.6$ eV, however, the calculated and experimental spectra are in excellent agreement with each other. The neutral distributions are considerably broadened by this correction since many of the ejecting low energy atoms are pulled back to the solid by the image force. The higher energy particles, then, make up a greater percentage of the distribution. In addition, the shapes of the ion distributions are a sensitive function of the polar collection angle, both in terms of the peak energy and the magnitude and shape of the high energy tails. Of particular interest is the $\theta=75°$ spectrum which exhibits the narrowest distribution. Examination of many individual trajectories from the calculation indicates that the reason for this shape is that ejecting Ni atoms with high polar angles are blocked in the ⟨100⟩ directions by next-nearest neighbor surface Ni atoms. The effect of the blocking is to produce a polar angle distribution (see Fig. 7) which essentially drops to zero with $\theta>65°$. Therefore, the low energy particles at $\theta=75°$ were originally ejected at smaller polar angles, but were bent into the detector by the image force. The effect of E_{image} on the higher kinetic energy particles will be much smaller and hence the $\theta=75°$ spectrum exhibits no high energy tail in its distribution.

The apparent signal-to-noise ratio of the calculated Ni^+ ion spectra is much lower than that of the neutral species. The reason for this decrease is that a large number of low energy particles cannot overcome the image potential and are pulled back to the solid dramatically reducing the total count. Subsequent normalization of the remaining Ni^+ intensity amplifies the signal variations in the high energy region where a relatively low number of particles are found to eject. For example, although ~1400 impact points were computed for the Ni(001)c(2×2)–CO system, the peak intensity in the $\theta=30°$ spectrum is only 40 counts after applying the image force correction.

Within the constraints of the statistical reliability of the data and the calculations, we feel the agreement is quite satisfactory. It is of interest that values of E_{image} outside the range of 3.6±0.3 eV yield very poor agreement with experiment for at least one of the polar angles. It is also of interest that, although we can fit our calculated data modified by Eq. (1) to the energy distribution obtained at $\theta=45°$ using $A/a=1.1\times10^6$ cm/s, we cannot find any value of A/a that is consistent with energy distributions obtained at the other polar angles. Our conclusion at this stage, then, is that a relatively strong image force is influencing ion trajectories, and that the differences between neutral and ion energy spectra can be rationalized using only E_{image} and not using relationships of the form of Eq. (1). If this picture is to be believed, however, our model must also predict both polar and azimuthal ion distributions and must also address the question of cluster formation. It is these topics to which we move next.

E. Comparison of calculated and observed angular distributions

As mentioned earlier, both the azimuthal and polar angle dependence of the Ni^+ signal was measured for the Ni(001)c(2×2)–CO surface. Of the two measurements, polar spectra should be most sensitive to the magnitude of E_{image} since the image force acts only on the perpendicular velocity component. In Fig. 7 we compare the observed polar dependence of Ni^+ ions ejected at 7±2 eV along the $\phi=0°$ azimuth to the predicted neutral and ion (neutral plus image correction) distributions. The experimental curve reaches maximum intensity at ~52° with a FWHM of 35°, while the predicted neutral distribution peaks at $\theta=39°$ with a FWHM of 29°. When the neutral distribution is corrected for $E_{image}=3.6$ eV, however, the angle of maximum yield shifts by about 10° to coincide with the experimental results.

Slightly different behavior is exhibited by Ni atoms with 22±2 eV kinetic energy as shown in Fig. 8. The

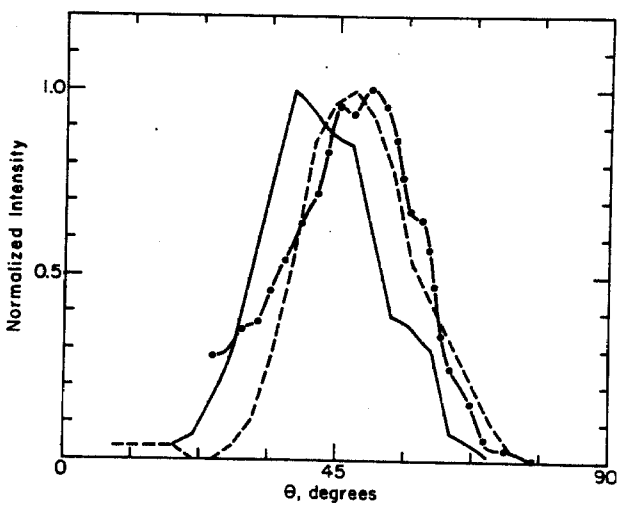

FIG. 8. Polar angle distributions for Ni ejected from Ni(001)c(2×2)–CO. Experimental conditions and codings are the same as for Fig. 6. The curves are recorded by selecting only those particles with 22±2 eV kinetic energy.

predicted peak maximum of the neutrals shifts from $\theta = 39°$ to $\theta = 47°$ with a FWHM of 22° when $E_{image} = 3.6$ eV is included. Of particular interest is that the FWHM is considerably smaller at the higher kinetic energies (22° vs 35°) due to the greater angular anisotropy observed under these conditions. This anisotropy arises since the higher kinetic energy particles leave the surface early in the collision cascade while the surface structure is still intact. Their ejection directions are then more susceptible to channeling by atoms in the top layer of the solid. The attenuation of Ni^+ intensity at high polar angles (>60°) shown in Fig. 8 is due to the next-nearest neighbor scattering mechanism discussed in the previous section.

The polar angle distributions for low kinetic energy ions (7±2 eV) ejected along $\phi = 45°$ are shown in Fig. 9. The maximum ion intensity for both experimental (36°) and predicted (38°–44°) ion curves are at lower values than in the $\phi = 0°$ polar plots. This effect is predicted by the dynamics calculations which show scattering from nearest-neighbor atoms in the surface at $\phi = 45°$ to be predominantly responsible for the observed structure. This same mechanism gives rise to the $\phi = 45°$ minima observed in the azimuthal plots for polar angles greater than about 25°. It should also be noted that at both $\phi = 0°$ and at $\phi = 45°$, application of Eq. (1) shifts the neutral curve closer to the normal regardless of the value of A/a.

Information contained in azimuthal angular spectra is more sensitive to surface structure than either the polar or energy distributions.[14,41] In addition, the azimuthal spectra obtained at large polar angles should be strongly influenced by any image force, since the image force acts to bend particles originally ejected at smaller polar angles into the detector. In Fig. 10, the azimuthal angular spectra obtained for 3±3 eV Ni^+ ions ejected at $\theta = 30°$, 45°, 60°, and 70° from Ni(001)c(2×2)–CO are shown. Predicted neutral and image force corrected distributions are also shown,

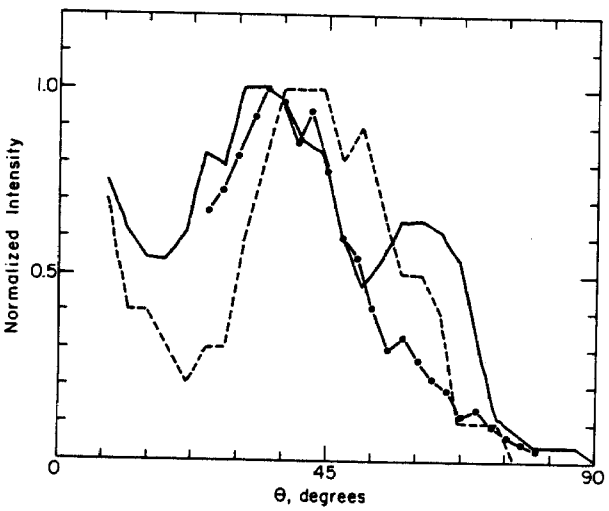

FIG. 9. Polar angle distributions for Ni ejected from Ni(001)c(2×2)–CO. Conditions are the same as for Fig. 7 except that $\phi = 45°$.

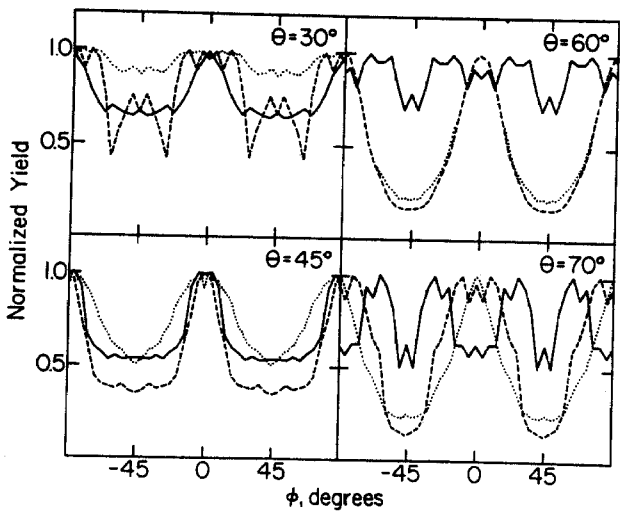

FIG. 10. Dependence of Ni^+ ion yield on azimuthal angle at various polar angles for Ni(001)c(2×2)–CO. The curve codings and experimental conditions are the same as for Fig. 6. Only those particles with 3±3 eV were detected.

again derived assuming the same E_{image} value of 3.6 eV. The $\theta = 30°$ experimental spectrum is only slightly anisotropic due to the relative lack of importance of the nearest-neighbor scattering mechanism and the fairly poor azimuthal angular resolution at near normal incidence ejection angles. Detailed comparison with the dynamics calculations is not possible in this case due to poor statistics. At $\theta = 45°$, both theoretical and experimental curves exhibit a higher anisotropy, although the predicted curve is somewhat more anisotropic than observed. Excellent agreement is seen in the $\theta = 60°$ curves, where maximum anisotropy is normally observed. Some splitting of the $\phi = 0°$ peak is predicted in the $\theta = 70°$ spectrum, presumably due to scattering of the emerging Ni^+ ions by next-nearest neighbor nickel atoms or adsorbed CO. However, it is not observed in the corresponding experimental distribution, which is sharply peaked at $\phi = 0°$.

In the course of determining an appropriate value of E_{image} for the energy and angle distributions, it was noted that in some cases changes in this parameter of as little as 0.2 eV significantly affected the resulting predicted spectra. The self-consistency of each of the best fit spectra ($E_{image} = 3.6$ eV was assumed in each) and the multidimensional nature of the data provide convincing evidence that the image force is playing an important part in determining ion trajectories. Although our estimate of the image interaction gives no direct information about the nature or kinetics of the ionization process, it does suggest some spatial limits on the position of the ejected particle as the secondary ion is formed. Thus, it may prove valuable as a test of ionization models which specify these parameters.

It is of interest to compare the azimuthal spectra for Ni(001)c(2×2)–CO to that of the clean Ni(001) surface to specifically measure the effect of the CO molecule on the ejecting Ni atom. Experimentally, it is very difficult to record ion signals from the clean metal surface, since

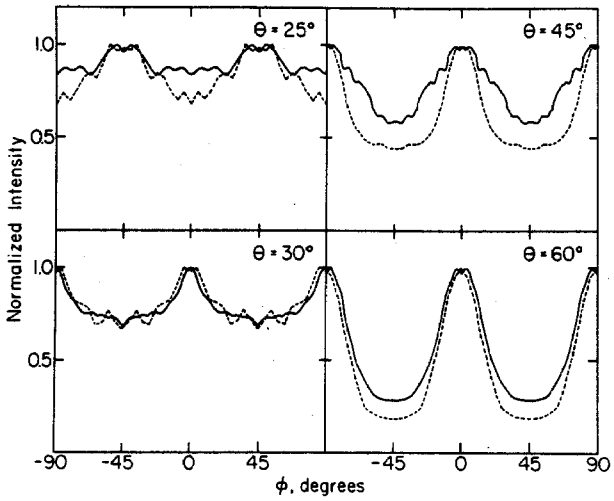

FIG. 11. Dependence of Ni^+ ion yield on azimuthal angle at various polar angle for clean Ni(001) bombarded by 1500 eV Ar^+ ions at normal incidence. The solid curves represent experimental data while the dashed curves are predicted values obtained by correcting the calculated yields for 1000 eV Ar^+ ion bombardment for the presence of the image force. Only those particles with a kinetic energy of 4 ± 4 eV were detected.

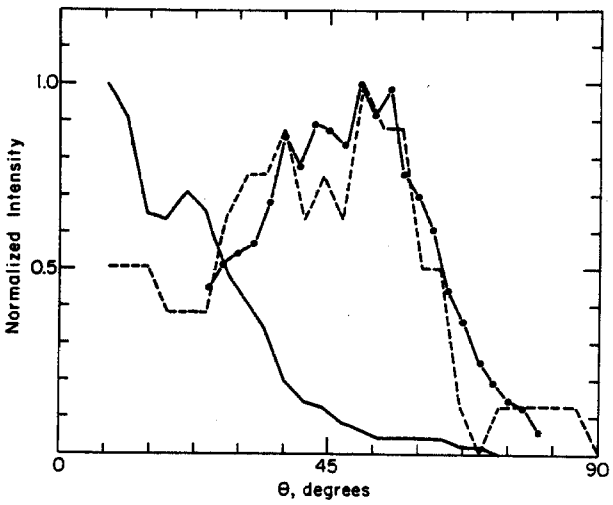

FIG. 12. Dependence of Ni_2^+ ion yield on polar angle for Ni(001)c(2×2)–CO bombarded by 1000 eV Ar^+ ions at normal incidence. The codings are the same as those given in Fig. 6. Only those particles with a kinetic energy of 3 ± 3 eV were detected.

the ion yield approaches zero in the limit of a perfectly clean surface and is very sensitive to even the smallest levels of impurities. Nevertheless, we have obtained azimuthal spectra for a surface estimated to contain less than 5% of a monolayer of oxygen or carbon containing impurities. The results are shown in Fig. 11 for $\theta = 25°$, 30°, 45°, and 60°. A somewhat smaller value of $E_{image} = 2.4$ eV yields the best fit between theory and experiment. In this case, we have compared experiments using 1500 eV Ar^+ ions to calculations using 1000 eV Ar^+ ions. We believe this comparison is justified due to the insensitivity of the angle and energy spectra to incident ion energies above values of several hundred eV, as discussed previously and shown in Fig. 3.

For clean Ni(001), the $\theta = 25°$ curve is of interest due to the maximum ion intensities observed at $\phi = \pm 45°$. Two main factors apparently contribute to this behavior: the nearest-neighbor scattering mechanism which attenuates $\phi = 45°$ ejection at higher polar angles does not affect these particles, and certain Ar^+ impact points lead to efficient momentum transfer along $\phi = 45°$ close packed rows, followed by glancing collisions which lead to ejection of low energy Ni^+ ions earlier in the trajectory sequence. The $\theta = 30°$, 45°, and 60° curves are similar to those obtained from the CO saturated surface.

Azimuthal spectra were also measured for higher kinetic energy (18 ± 4 eV) Ni^+ secondary ions ejected from both clean and Ni(001)c(2×2)–CO. They exhibit behavior similar to the corresponding low energy curves, with slightly greater anisotropy noted at each polar angle as observed for the CO covered surface. Comparison to theory is hampered by the low number of particles and consequent poor statistical significance of the predicted ion distributions.

F. Angular and energy dependence of multimer ion yields

The spatial and energy distributions of Ni_2^+ and $NiCO^+$ ions ejected from the Ni(001)c(2×2)–CO surface by 1500 eV Ar^+ ions were also investigated in an attempt to gain further information about particle ejection, cluster formation, and secondary ionization processes. Multimer ions detected by SIMS are predicted to be indirectly related to the original surface geometry of the constituent atoms[16,30] and can give information about the ejection mechanism of species which cannot be directly measured by the SIMS technique. For example, recent molecular dynamics calculations indicate that ~85% of the CO particles ejected from the saturated Ni(001) surface remain

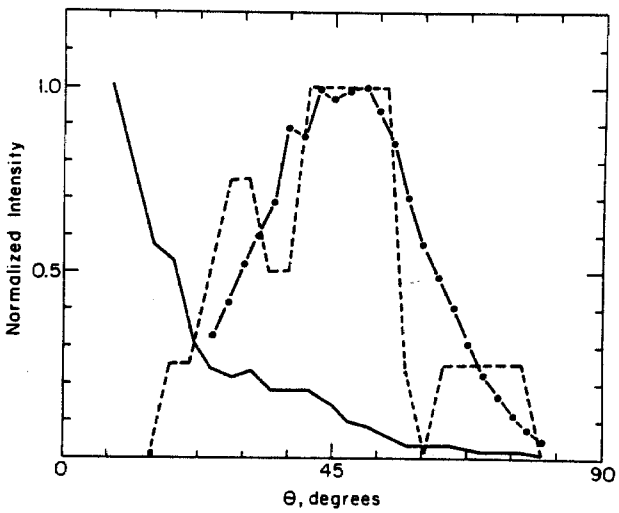

FIG. 13. Dependence of $NiCO^+$ ion yield on polar angle for Ni(001)c(2×2)–CO bombarded by 1000 eV Ar^+ ions at normal incidence. The codings are the same as those given in Fig. 6. Only those particles with a kinetic energy of 3 ± 3 eV were detected.

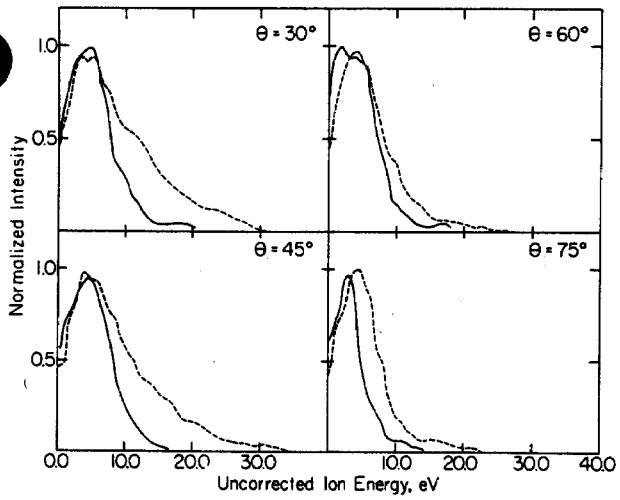

FIG. 14. Uncorrected secondary ion kinetic energy distributions of Ni_2^+ (- - - - -) and $NiCO^+$ (——) ions ejected from Ni(001)c(2×2)–CO at $\phi = 0°$. The analyzer bandwidth was approximately 4 eV.

intact, and some fraction of these may interact in the near surface region to form NiCO and other multimers.[16] Although CO^+ ions are not detected in the SIMS experiment, presumably due to the molecule's high ionization potential,[1] careful evaluation of the $NiCO^+$ data from the SIMS experiment may allow inference of the CO ejection angles with the aid of the dynamics calculation.

The measured polar angle distributions of Ni_2^+ and $NiCO^+$ are shown in Figs. 12 and 13, respectively. Data from the two spectra are remarkably similar, showing broad maxima centered around 51° for Ni_2^+ and 47° for $NiCO^+$. These low kinetic energy (3 ± 3 eV) multimers also exhibit significant intensity at high polar angles, similar to that observed for the nickel monomer ion (Fig. 7). The calculated Ni_2^+ ion distribution agrees well with the experimental data using $E_{image} = 3.4$ eV in spite of the low number of particles predicted after correction for the image potential. However, the value of E_{image} must be increased to 5.8 eV to achieve a reasonable fit with the $NiCO^+$ data. This seems surprising since the evidence accumulated thus far suggests that formation of the $NiCO^+$ ion occurs from the interaction of a Ni^+ ion with a CO molecule. Thus, we would expect the image potential for $NiCO^+$ to be comparable to that calculated for Ni^+ ions. Efforts are currently underway to develop a more sophisticated treatment of the ionization/cluster formation processes in the dynamics calculation which may explain this result and ultimately provide information about the mechanism and time sequence of these processes. At this point, we believe it prudent to not over-interpret the significance of the actual value of E_{image}.

The energy spectra of Ni_2^+ and $NiCO^+$ ions measured at $\theta = 30°$, 45°, 60°, and 75° at $\phi = 0°$, are shown in Fig. 14. As expected, the multimer species exhibit a much narrower energy distribution than is observed for Ni^+ ions. This reflects the low probability for two relatively fast moving particles produced from a single Ar^+ ion impact to have sufficiently low relative kinetic energies to form multimers. The effect is most dramatic in the $NiCO^+$ spectra. Apparently, high energy Ni and CO particles arise from fundamentally different ejection mechanisms and are almost never ejected in similar directions. It is somewhat more probable that two high energy Ni particles may be ejected in spatially similar trajectories,[23,30] leading to the weak high energy tail observed in the Ni_2^+ spectra at 30° and 45°. Unfortunately, a detailed comparison of these spectra to predicted energy distributions is precluded by the extremely low number of multimer ions observed in the trajectory calculations.

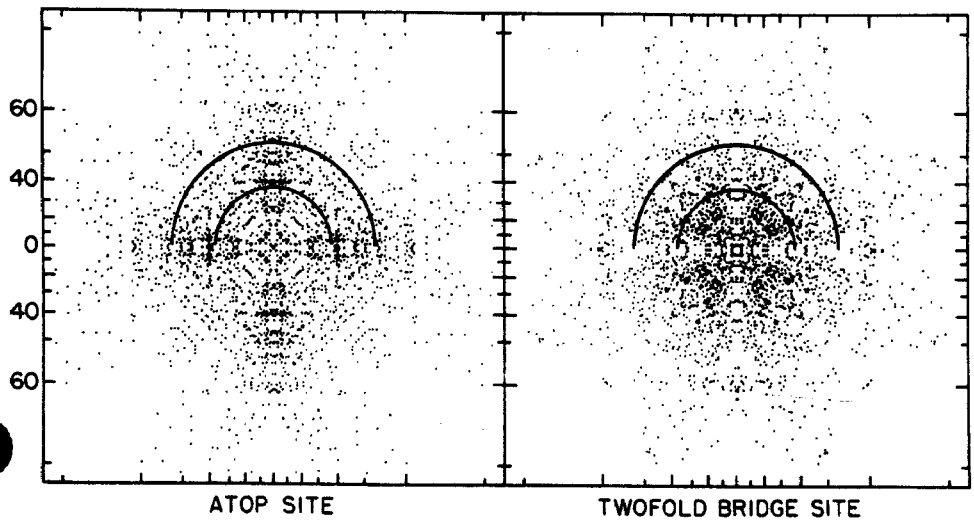

FIG. 15. Predicted angular distributions of Ni^+ ion intensity for the CO adsorbed in atop and twofold bridge sites. The numbers on the ordinate refer to the polar deflection angle given in degrees. The display is oriented the same as Fig. 1 so that the horizontal and vertical directions correspond to $\phi = 0°$. The points between the circles contribute to the azimuthal distribution at $\theta = 45 \pm 7°$ in Fig. 16. Only those particles with kinetic energies of 3 ± 3 eV were counted.

G. Comparison between the predicted angular distributions for the CO in atop and twofold bridge sites

The calculations have suggested that the angular distributions of the ejecting particles should reflect the geometry of the atoms in and on the surface. Of interest here is how the CO bonding site, either atop or twofold bridge, influences the ejection directions of the Ni^+ ions. The angular distributions of the ejecting CO molecules would probably exhibit the strongest effect, but unfortunately they cannot be detected experimentally. Shown in Fig. 15 are the calculated total angular distributions of Ni^+ ions ejected from crystals with CO molecules in the two different sites. In this representation each ejecting particle's ultimate position is represented by a dot on a flat plate collector a large distance above the surface. The radial extent of a point is proportional to the tangent of the polar angle θ. The same data are plotted as azimuthal distributions in Fig. 16. The kinetic energy range of the secondary ions is 3 ± 3 eV and an image force correction of 3.6 eV has been included. The azimuthal distribution curves for the atop site are identical to those in Fig. 10.

Upon examination of either the flat plate collector displays or the azimuthal distributions, obvious differences are apparent. For example, at a polar angle of 45° the atop distribution is quite anisotropic, peaking in the $\phi = 0°$ direction. In contrast, from the twofold bridge distribution the Ni^+ ion intensity is virtually isotropic.

As stated above, it would be easier to make definitive geometry determinations if we could directly detect the ejected CO intensity. For example, although the calculated Ni^+ azimuthal distributions are different with the CO in atop or twofold bridge sites, the distributions from the atop site (Fig. 10) are similar to those from the clean metal (Fig. 11).

V. CONCLUSION

We have presented experimental SIMS results for Ni^+ ions ejected from a well-defined Ni(001)c(2×2)–CO surface. By constructing an apparatus capable of measuring ion yields at specific angles and energies, we have been able to make more direct comparisons to predictions of proposed models of the ion bombardment process. Clearly, these types of comparisons are critically needed if the SIMS spectra are ever to be explained in a quantitative fashion. Of special interest is that our experimental measurements agree well with calculated values over a wide range of experimental conditions, if the calculated results are modified by the inclusion of a strong image force.

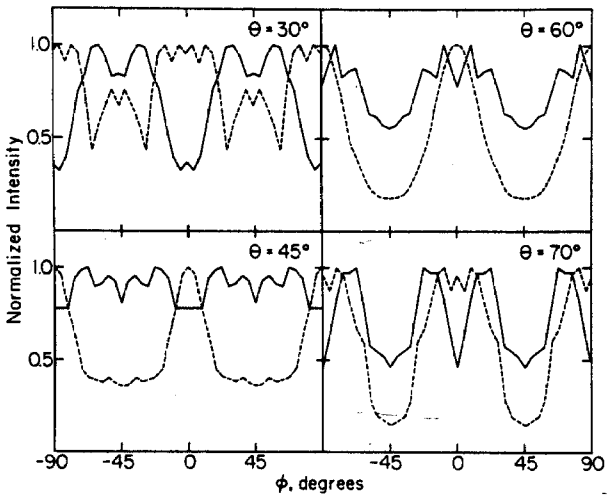

FIG. 16. Predicted azimuthal dependence of the Ni^+ ion yield for Ni(001)c(2×2)–CO for CO adsorbed in atop (- - - - -) and twofold bridge sites (——). Only those particles with kinetic energies of 3 ± 3 eV were counted.

This high level of agreement is somewhat surprising since the correct form of the appropriate scattering potentials utilized in the classical dynamics model are not known. We have completed some testing employing other forms of the potential than those reported earlier.[42] For example, using a Molière potential[43] to describe the Ar–C, Ar–O and Ar–Ni interaction, we obtained nearly identical results, except under conditions where the statistical reliability was low and at near normal polar angles ($\theta \leq 25°$). The potential parameters for the atoms in the solid have also been shown to influence the trajectory. For example, both the location of the atoms[44] and their relative sizes[45] are important factors in influencing both polar and azimuthal angle plots. In our case, of course, the initial atomic locations have been determined using other techniques, and we must conclude that the model is accurate enough to provide physically reasonable results.

We believe the comparisons presented here provide a number of severe constraints for proposed ionization theories. The value of R^+ should be only weakly dependent on velocity and should be nearly isotropic. We cannot explain our results using the Auger neutralization scheme which is valid for incoming ions of fairly low energy.[34]

Finally, it is hoped that these studies will provide part of the basis for employing angle resolved SIMS in the determination of surface structures. We have suggested previously that large differences exist between adsorbates bound in atop or fourfold bridge geometries and have demonstrated this prediction at least qualitatively. In this paper, we have shown there are major predicted differences between the atop bonded CO and the twofold bridge bonded CO. As more information about the surface ionization process and about the details of the forces acting between the atoms becomes available, we hope the applicability of the approach will broaden.

ACKNOWLEDGMENTS

The authors wish to thank the National Science Foundation, the Office of Naval Research, the Air Force Office of Scientific Research and the Petroleum Research Foundation administered by the American Chemical Society for financial support. One of us (BJG) also acknowledges the A. P. Sloan Foundation for a Research Fellowship and the Camille and Henry Dreyfus Foundation for a grant for newly appointed young faculty.

[1] T. Fleisch, G. L. Ott, W. N. Delgass, and N. Winograd, Surf. Sci. **81**, 1 (1979).

[2]P. H. Dawson and W. Tam, Surf. Sci. **91**, 153 (1980).
[3]R. S. Bordoli, J. C. Vickerman, and J. Wolstenholme, Surf. Sci. **85**, 244 (1979).
[4]H. Hopster and C. R. Brundle, J. Vac. Sci. Technol. **16**, 548 (1979).
[5]P. H. Dawson, Surf. Sci. **71**, 247 (1978).
[6]M. L. Yu, Surf. Sci. **71**, 121 (1978).
[7]D. E. Harrison, Jr., P. W. Kelly, B. J. Garrison, and N. Winograd, Surf. Sci. **76**, 311 (1978).
[8]N. Winograd, D. E. Harrison, Jr., and B. J. Garrison, Surf. Sci. **78**, 467 (1978).
[9]B. J. Garrison, N. Winograd, and D. E. Harrison, Jr., Phys. Rev. B **18**, 6000 (1978).
[10]N. Winograd, B. J. Garrison, and D. E. Harrison, Jr., Phys. Rev. Lett. **41**, 1120 (1978).
[11]N. Winograd, K. E. Foley, B. J. Garrison, and D. E. Harrison, Jr., Phys. Lett. A **73**, 253 (1979).
[12]N. Winograd, B. J. Garrison, T. Fleisch, W. N. Delgass, and D. E. Harrison, Jr., J. Vac. Sci. Technol. **16**, 629 (1979).
[13]B. J. Garrison, N. Winograd, and D. E. Harrison, Jr., Surf. Sci. **87**, 101 (1979).
[14]S. P. Holland, B. J. Garrison, and N. Winograd, Phys. Rev. Lett. **43**, 220 (1979).
[15]Z. Sroubek, K. Zdansky, and J. Zavadil, Phys. Rev. Lett. **45**, 580 (1980).
[16]N. Winograd, B. J. Garrison, and D. E. Harrison, Jr., J. Chem. Phys. **73**, 3473 (1980).
[17]D. J. Auerbach, C. A. Becker, J. P. Cowin, and L. Wharton, Rev. Sci. Instrum. **49**, 1519 (1978).
[18]R. A. Gibbs and N. Winograd, Rev. Sci. Instrum. **52**, 1148 (1981).
[19]J. C. Tracy, J. Chem. Phys. **56**, 2736 (1972).
[20]K. Akimoto, Y. Sakisaka, M. Nishimima, and M. Onchi, Surf. Sci. **88**, 109 (1979).
[21]M. Passler, A. Ignatiev, F. Jona, D. W. Jepsen, and P. M. Marcus, Phys. Rev. Lett. **43**, 360 (1979).
[22]S. Andersson and J. B. Pendry, Phys. Rev. Lett. **43**, 363 (1979).
[23]K. E. Foley and B. J. Garrison, J. Chem. Phys. **72**, 1018 (1980).
[24]K. Wittmaack, Surf. Sci. **53**, 626 (1975).
[25]Z. Sroubek, Surf. Sci. **44**, 47 (1974).
[26]P. H. Dawson, Surf. Sci. **57**, 229 (1976).
[27]A. R. Krauss and D. N. Gruen, Nucl. Inst. Methods **149**, 547 (1978).
[28]R. G. Hart and C. B. Cooper, Surf. Sci. **94**, 105 (1980).
[29]K. E. Foley, B. J. Garrison, and N. Winograd (to be published).
[30]S. P. Holland, B. J. Garrison, and N. Winograd, Phys. Rev. Lett. **44**, 756 (1980).
[31]W. F. van der Weg and D. N. Bierman, Physica **44**, 177, 206 (1969).
[32]A. Benninghoven, Surf. Sci. **35**, 457 (1973).
[33]H. D. Hagstrum, in *Inelastic Ion-Surface Collisions*, edited by N. H. Tolk, J. C. Tully, W. Heiland, and C. W. White (Academic, New York, 1977), p. 1.
[34]H. D. Hagstrum, J. Vac. Sci. Technol. **12**, 7 (1975).
[35]K. Wittmaack, in *Inelastic Ion-Surface Collisions*, edited by N. H. Tolk, J. C. Tully, W. Heiland, and C. W. White (Academic, New York, 1977), p. 153.
[36]Z. Sroubek, J. Zavadil, F. Kubec, and K. Zdansky, Surf. Sci. **77**, 603 (1978).
[37]P. Williams, Surf. Sci. **90**, 588 (1980).
[38]J. Bardeen, Phys. Rev. **58**, 727 (1940).
[39]J. K. Norskov and B. I. Lundquist, Phys. Rev. B **19**, 5661 (1979).
[40]J. A. Applebaum and D. R. Hamann, Phys. Rev. B **6**, 1122 (1972).
[41]N. Winograd and B. J. Garrison, Acc. of Chem. Res. **13**, 406 (1980).
[42]N. Winograd, D. E. Harrison, Jr., and B. J. Garrison (to be published).
[43]I. M. Torrens, *Interatomic Potentials* (Academic, New York, 1972).
[44]S. Kapur and B. J. Garrison, J. Chem. Phys. **75**, 445 (1981).
[45]S. Kapur and B. J. Garrison, Surf. Sci. **109**, 435 (1981).